Global Journal of Science Frontier Research: H
Environment & Earth Science
Volume 21 Issue 4 Version 1.0 Year 2021
Type: Double Blind Peer Reviewed International Research Journal
Publisher: Global Journals
Online ISSN: 2249-4626 & Print ISSN: 0975-5896

Copper Decorated on Fluorine Doped Tin Oxide as a Transparent Conductor Oxide for Photovoltaic Energy by DSSCs

By Edwalder Silva Teixeira, Francisco Marcone Lima, Vanja Fontenele Nunes, Antonio Paulo Santos Souza, Ana Fabíola Leite Almeida & Francisco Nivaldo Aguiar Freire

Laboratory of Thin Films and Renewable Energy - LAFFER/UFC

Abstract- In this work, films of fluorine doped tin oxide (FTO) with and without copper have been successfully synthesized by spray pyrolysis on conductive transparent substrates without acid addition. Sprayed film samples were used in the determination of photovoltaic parameters in the dye-sensitized solar cells (DSSCs), including open-circuit voltage (Voc), short circuit current density (Jsc), fill factor (FF), efficiency (η), shunt (Rshunt) and serial (Rserial) resistances. Characterization techniques determined the sheet electrical resistance, optical transmittance, thickness, band gap, topographical and structural characterizations, and flat-band potential of the sprayed films. The X-rays diffraction showed peak distribution of the sprayed products similar to the tin dioxide phase. There was morphological change, with smaller and more compact grains by adding copper. Also, conduction band edge, sheet resistance, optical transmittance and optical band gap change as function of the amount of copper.

Keywords: spray pyrolysis, characterization, photovoltaic, environmental.

GJSFR-H Classification: FOR Code: 090608

Copper Decorated on Fluorine Doped Tin Oxide as a Transparent Conductor Oxide for Photovoltaic Energy by DSSCs

Edwalder Silva Teixeira [α], Francisco Marcone Lima [σ], Vanja Fontenele Nunes [ρ], Antonio Paulo Santos Souza [ω], Ana Fabíola Leite Almeida [¥] & Francisco Nivaldo Aguiar Freire [§]

Abstract- In this work, films of fluorine doped tin oxide (FTO) with and without copper have been successfully synthesized by spray pyrolysis on conductive transparent substrates without acid addition. Sprayed film samples were used in the determination of photovoltaic parameters in the dye-sensitized solar cells (DSSCs), including open-circuit voltage (Voc), short circuit current density (Jsc), fill factor (FF), efficiency (η), shunt (Rshunt) and serial (Rserial) resistances. Characterization techniques determined the sheet electrical resistance, optical transmittance, thickness, band gap, topographical and structural characterizations, and flat-band potential of the sprayed films. The X-rays diffraction showed peak distribution of the sprayed products similar to the tin dioxide phase. There was morphological change, with smaller and more compact grains by adding copper. Also, conduction band edge, sheet resistance, optical transmittance and optical band gap change as function of the amount of copper. After the characterization, fluorine doped tin oxide films with and without copper, on transparent substrate, were used in the dye-sensitized solar cells assembly. The results showed this methodology as an environmentally friendly way for preparation, characterization and application of copper decorated FTO films in photovoltaic devices. The aim of this work is to divulge the results on the copper decorated SnOx: F sprayed films obtained from the techniques cited applied in DSSCs.

Keywords: spray pyrolysis, characterization, photovoltaic, environmental.

I. Introduction

Transparent electrical conductor materials (TECMs) can be of various structures, such as oxides. Fluorine doped tin oxide (FTO) semiconductors as well as oxides mixtures, non-oxides and organic materials using acidic solutions can be cited as examples [1, 2]. TECMs are unique, exhibiting both transparency and electrical conductivity.[1] The interest on TECMs for application in the interfacial charge transfer process, in particular the photovoltaic area, has been growing in the last years due to their unique characteristics.

Author α σ ρ ω ¥ §: Laboratory of Thin Films and Renewable Energy – LAFFER/UFC, (Avenida Humberto Monte S/N, Campus do Pici, 60455-900), Fortaleza, Ceará Brazil. e-mails: edwalderteixeira@hotmail.com, marconeufc@gmail.com, vanjafnunes@gmail.com, antonio.souza@fisica.ufc.br, anfaleal@yahoo.com.br, nivaldo@ufc.br

The material properties are affected by doping. The choice of dopants must be done to minimize the net distortion and preserve the phase [1]. Therefore, the structural, electrical and optical properties of tin dioxide (SnO_2) semiconductor have been tailored by dopants such as fluorine (F) [3-9], antimony (Sb) [8], molybdenum (Mo) [10], manganese (Mn) [11], copper (Cu) [12] and chromium (Cr) [13].

The fluorine doped tin oxide semiconductor film is one TECM typically used in the dye-sensitized solar cells (DSSCs) assembly [14-31]. Fluorine doped tin oxide (SnO_x:F) films have been made from inexpensive raw materials, using simple spray pyrolysis technique [3,8]. The "x" superscript in the chemical formula indicates the absence of oxygen atoms, i.e, stoichiometric deviation. The oxygen holes combined with the fluorine (F) doping are the key to the electrical conductivity and transparency in SnO_x: F films [1, 32].

The two points method associated with the Equation 1 has been used in the electrical characterization of films by sheet electrical resistance (R_s) measurements [3, 5, 33]. In SnO_x: F films deposited by spray pyrolysis technique, equation (1) is used for measurement of the R_s, from electrical resistance (R) value measured by digital multimeter [5]. Besides the R_s measurements, the films have been characterized by superficial morphology [14, 15, 20] and thickness [5, 17, 22] by scan electron microscopy (SEM).

$$R_s = \frac{\rho}{t} = R\left(\frac{W}{L}\right) \quad (1)$$

where ρ is the electrical resistivity, t is the film thickness, W is the width, L is the length and the ρ/t ratio is called sheet resistance (R_s).

The UV-vis spectroscopy has been usually employed as a tool for the optical characterization of materials through transmittance [9-12, 35]. The determination of the band gap (E_g) value by the Tauc method (Equation 2,3) using optical transmittance data has been reported [4,6,9,10,13,36]. Also, the thickness determination (t) from optical transmittance was reported [7, 35]. Additionally, Equations (4, 5 and 6)

Global Journal of Science Frontier Research (H) Volume XXI Issue IV Version I Year 2021
1

were used as tool to determine t, using optical transmittance data [7].

$$\alpha hv = t\left(hv - E_g\right)^i \quad (2)$$

$$\alpha = -\frac{1}{t}\ln(T) \quad (3)$$

where h: Planck constant, v: light frequency, which is the ratio between the light speed constant and the wavelength (λ), i = 1/2 (direct transition semiconductor) and i = 2 (indirect transition semiconductor), α: absorption coefficient, T: transmittance data and t: film thickness.

$$C(\lambda) = \frac{T^+(\lambda) - T^-(\lambda)}{2T^+(\lambda)T^-(\lambda)} \quad (4)$$

$$n_{film}(\lambda) = \frac{\left[8n_{sub}C(\lambda) + (n_{sub}+1)^2\right]^{1/2} + \left[8n_{sub}C(\lambda) + (n_{sub}-1)^2\right]^{1/2}}{2} \quad (5)$$

$$t = \left(2\left[\frac{n_{film}(\lambda_1)}{\lambda_1} - \frac{n_{film}(\lambda_2)}{\lambda_2}\right]\right) \quad (6)$$

where, n_{film}: film refractive index, n_{sub}: substrate refractive index, $T^+(\lambda)$ and $T^-(\lambda)$ are transmittance values in the peak top and bottom at each wavelength (λ), respectively.

By X-ray diffraction (XRD) characterization, the SnO_x:F films manufactured by the spray pyrolysis technique, which commonly has addition of acid, have been characterized as a pure stoichiometric tin oxide (SnO_2) phase [4-8]. The absence of the SnO_x: F phase has been attributed to the dopant nature of the fluorine (F) and the oxygen vacancies, where their concentration in sprayed films are below the detection limit of the XRD equipment. Thus, SEM, UV-vis spectroscopy and other techniques have been combined with XRD to help characterize sprayed films as SnO_x:F.

Additionally, the electrochemical characterization studies the interfacial charge transfer process from between two or more materials junctions. The electrochemical methods have been used as tools to derive properties of semiconductors from the interfacial charge transfer processes [29, 30]. The determination of the SnO_2 and titanium dioxide (TiO_2) conduction bands from flat-band potential (E_{fbp}) obtained by Mott-Schottky electrochemical method was report elsewhere [39].

The semiconductor characterization in n-type or p-type has been made by electrochemical technique called Mott-Schottky through the electrochemical cell with three electrodes and an electrolyte [20,23,36,40-44]. The electrochemical capacitance (C) of the semiconductor/electrolyte junction as function of potential applied (E) is given by the Mott-Schottky equation (7) [36,40-44].

$$\frac{1}{C^2} = \frac{2}{\varepsilon_\infty \varepsilon_r A^2 N}\left(E - E_{fbp} - \frac{k_b T}{q}\right) \quad (7)$$

where ε_∞ (8.854 x 10^{-14} F cm^{-1}): permittivity of free space, ε_r: relative dielectric constant of the specimen, A(cm^2): sample area, N (cm^{-3}): electrons donor (n-type semiconductor) or electrons acceptor (p-type semiconductor) density, E (V): applied potential, E_{fbp} (V): band potential, k_b (1.38 x 10^{-23} J K^{-1}): Boltzmann constant, T (K): absolute temperature and q (1.602 x 10^{-19} C): the electron charge.

The study of the influence of copper (Cu) atoms in the SnO_x: F sprayed film properties and their impact on photovoltaic characteristics of DSSCs has not been reported in the literature. From this scenario, the aim of this work is to divulge the results of the copper decorated SnO_x:F sprayed films obtained from the techniques cited in the review above. Also, sprayed films samples were used in the determination of photovoltaic parameters of DSSCs, including open-circuit voltage (V_{oc}), short circuit current density (J_{sc}), fill factor (FF), efficiency (η), shunt (R_{shunt}) and serial (R_{serial}) resistances.

II. Materials and Methods

a) *Obtaining the sprayed films*

A muffle furnace (EDG F-1800) with ceramic heater (220V/500W, Higher) was used for calcination. The heating rate was 7 °C/min and the work temperature at 600 °C. Microscopy glass were the substrates. The solutions were atomized into a fine droplet spray by nozzle (α4, APREX) with the help of an air carrier gas fed into the spray nozzle from the air compressor (Twister, SHULZ).

The starting materials were tin chloride II dihydrate ($SnCl_2.2H_2O$), ammonium fluoride (NH_4F), copper chloride II dehydrated ($CuCl_2.2H_2O$). All the reactants were purchased from Vetec. The solution with 10.00 g of $SnCl_2.2H_2O$, 1.65 g of NH_4F and 10.00 mL deionized water (H_2O) was named A and the sprayed product designated as SOF. The solutions with copper salt were designated as BX, where X = 1, 2, ... , 9 and the sprayed products obtained from the combination of the solutions A and BX were named as SOFC (Table 1).

For the formation of the SOFC products, the A and BX solutions were sprayed out of the furnace on the heated glass substrates, inside an exhaustion chamber. The spray was alternated (A,BX,A,BX,A,...) and after each spray the substrates were placed inside the furnace to apply the working temperature. The procedure was repeated until all the solutions were sprayed on the substrates. The SOF product was used as a reference sample for comparison with the ones modified by copper atoms.

Table 1: Chemicals and products.

$CuCl_2.2H_2O$ (g)	H_2O (mL)	SOLUTION BX	PRODUCT (SOFC)
0.10	5.00	B9	SOF C0.1
0.20	5.00	B8	SOF C0.2
0.30	5.00	B7	SOF C0.3
0.40	5.00	B6	SOF C0.4
0.50	5.00	B5	SOF C0.5
1.00	5.00	B4	SOF C1.0
1.50	5.00	B3	SOF C1.5
2.00	5.00	B2	SOF C2.0
2.50	5.00	B1	SOF C2.5

b) Sprayed films characterization

The phase identification of the materials deposited on the substrates was done by the X-Ray diffraction (XRD) technique with D8 Advance equipment (Buker). The measurement conditions were: copper (Cu) anode, radiation Cu-Kα λ = 1.54 Å, 40 kV, 45 mA, variation of 2θ from 5 ° to 100 °.

The films growth was characterized by the transversal area images obtained through scanning electron microscopy (SEM) using Quanta FEG equipment (FEI). The digital multimeter (Fluke) was used to measure the electrical resistance value (R). The electrical characterization by sheet resistance (Rs) was estimated from the two points method and Equation 1 using materials with dimensions about 2.50 cm x 2.50 cm.

The electrochemical characterization by Mott-Schottky (M-S) of sprayed films was done using a three electrodes electrochemical cell using the PGSTAT302N potentiostat/galvanos-tat (Metrohm, Switzerland). Work electrode was sprayed film; counter electrode was platinum (Pt) plate and silver/silver chloride (Ag/AgCl) as the reference. The sprayed films were about 2.50 cm x 1.0 cm with active area of 1.0 cm^2, which is the working electrode fraction in contact with the 50.00 mL aqueous solution of sodium hydroxide 1.0 molar (1.0 M NaOH).

The measurement conditions by the M-S technique were potential variation between -1.00 V up +1.00 V, 100000 Hz until 10 Hz frequency range, eleven points per decade and signal amplitude about 10.00 mV. Plots of the capacitance reciprocal against applied potential (1/C2 against E) were generated. The straight line inclination was used to classify the semiconductor in p-type (holes excess into valence band) or n-type (electrons excess into conductive band). The line extrapolation in the direction of the E magnitude was used to estimate the flat-band potential (Efbp).

For the optical characterization, it was used the UV-visible spectrophotometer (Cary 100, Agilent) in the transmittance mode between the wavelengths of 200 nm up to 800 nm. The determination of the thickness (t) and band gap (Eg) was obtained from the transmittance (T) against wavelength (λ) data. The t values were estimated using Equations 4, 5, and 6, while the Eg values were estimated from Equation 2. The adopted conditions for obtaining Eg were direct transition $(\alpha hv/t)^2$ against energy of the incident photon (hv) plot and data extrapolation to the condition (αhv/t)2 = 0.

c) Photovoltaic characterization: electrochemical and electrical

i. *Dye-sensitized solar cell assembly*

Sprayed film substrates were cleaned by the same volume ratio of water and ethanol alcohol mixture; in ultrasonic water bath (Q3360, Quimis) for 10 min. Subsequently, 0.084 g of SnO2 (99%, M) and 10% (mass/mass) SnO2-CuO (99%, Vetec) mixtures were prepared. All materials were added into volumes with 10 mL distilled water, then ultrasonic water bath for 10 min and stirring. Sprayed film substrates were added into the colloidal solution and the evaporation by natural convection happened for 7 days. All photoanodes with 0.5 cm2 active area were calcined at 450°C for 30 min in air atmosphere (EDG F-1800).

Photoanodes were immersed in equal volumes of solutions prepared from ethanol (Vetec), Ruthenizer 535-bisTBA(N719) dye and chenodeoxycholic acid into closed containers for 24 hours. These solutions were obtained from 7.50 mL of ethanol with 3.0 mg of N719 and 12.00 mg of acid. Platinum on fluorine-doped tin oxide (FTO) glasses were used as counter electrodes. The iodide/triiodide (I-/I3-) electrolyte (Iodolyte AN-50) was added onto the DSSC sandwich structures. The N719 dye, chenodeoxycholic acid and counter electrodes were obtained from Solaronix, Switzerland.

III. Characterization

In order to study the photovoltaic characteristics as a function of the sprayed films, the devices were characterized in terms of current density (J)-voltage (V).

The characterization was done using PGSTAT302N potentiostat/galvanostat and light source with LED generating 100 mW/cm2 white luminous energy. The system was controlled by computer through the NOVA1.10® program. The system and software (Solaronix, Switzerland) was specifically designed for DSSCs. From J-V, Voc, Jsc, FF, η, Rshunt and Rserial values were obtained.

IV. Results and Discussion

a) DRX

The oxygen vacancies (Vö) provide electrons transport in pure tin dioxide (SnO2) due the stoichiometric deviation, where the electrons generation can be described by equation 8.1 The understanding of the structural, optical and electronic properties of SnO2 films was improved by comparison between pure and doped SnO2 films [1, 32].

$$O^{--} \rightarrow V_{ö} + 2e + 1/2O_2(g) \qquad (8)$$

According to equation 8, when the oxygen anions escape as oxygen molecules (O2) out of the SnO2 from the oxygen anions (O--) occupied sites, it is created ionized vacant sites (Vö) and two free electrons. The Vö occurs due to the chemical diffusion process of the O-- in bulk stoichiometric SnO2 that results in SnO2-y, where y range about 0.02 until 0.034 from 700 K until 990 K temperature range 1. One other way, the pure SnO2 stoichiometric deviation can be described as Sn+4(1-δ)Sn+2δO-2(2-δ), where δ is the amount of vacant sites generated from the oxygen absence occupied by Sn+2 cations [32].

If we assume that the Sn+4(1-δ)Sn+2δO-2(2-δ) has doping by Sn+2, then it is valid the Sn+4(1-δ)O-2(2-δ):Sn+2δ formula. Thus, the SnO2-y and Sn+4(1-δ)Sn+2δO-2(2-δ) can be designated as SnOx for x= 2-y, as well as Sn symbol is a short representation for the Sn+4(1-δ)Sn+2δ with Sn+2 being the dopant of fraction (δ < y) or all (δ = y) of all oxygen vacancy sites. Besides the oxygen deficiency and Sn+2, dopants such as fluorine (F) [3-9], antimony (Sb) [8], molybdenum (Mo) [10], manganese (Mn) [11], copper (Cu) [12] and chromium (Cr) [13] have been used to modify the structural, optical and electrical properties of the SnO2 films.

The incorporation of Sb5+ in the Sn4+ sites and F-1 in the O-2 sites happens by substitution and it is accommodated in the SnO2 net. [1,8] It has been assumed that the fluorine doped-sprayed films identified by XRD as bulk pure SnO2 is an approximate measurement of the SnO2 films with presence of both stoichiometric deviation and fluorine into its structure [3-8].

In the fluorine doped stoichiometric deviation, SnO2 films obtained by spray pyrolysis from tin dichloride (SnCl2) and ammonium fluoride (NH4F) are generated from the tin oxide (SnO) and tin tetrafluoride (SnF4) transitory compounds [8]. Thus, the experimental data (Figure 1) obtained by X-rays diffraction (XRD) technique was used to identify the nature of the sprayed films called SOF and SOFC.

Figure 1 shows that the SOF and SOFC films have XRD peak distribution similar to the SnO2 and tin oxide fluoride (Sn4OF6) or SnO:(SnF2)3 equivalent, which are stoichiometric oxides. Both SOF and SOFC materials were identified as Sn4OF6 (ICSD 078356 sheet data) phase into $20^{o} < 2\theta < 70^{o}$ and into $60^{o} < 2\theta < 85^{o}$ as pure SnO2 (ICSD 039175 sheet data) phase. For SOF material, the similar XRD peak distribution in the $20^{o} < 2\theta < 85^{o}$ region was reported for SnO2 films with stoichiometric deviation and fluorine dopant obtained from $SnCl_2$ and NH_4F solutions using spray pyrolysis [7].

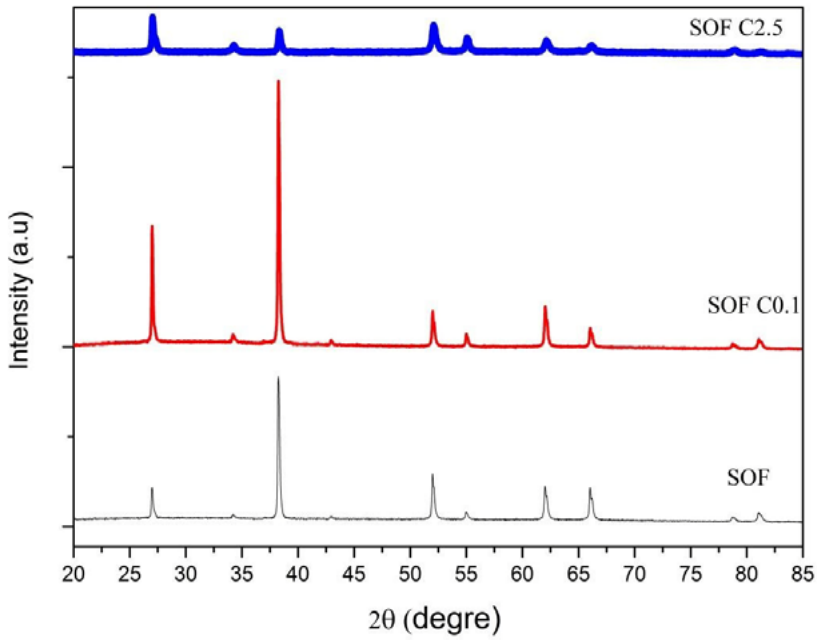

Figure 1: XRD of samples SOF and SOFC.

The spray pyrolysis creates oxides with stoichiometric deviation. Therefore, we can assume that SnO2 is an approximation of the SnOx:F, while that the SnO:(SnF2)3 could be replaced as SnOx:SnF2 or SnOx:(SnF2)y due to a stoichiometric deviation. Thus, SnOx:D is a general form for representation of SOF and SOFC materials, where D = F, SnF2 or (SnF2)y as possible dopants. The symbol "x" in SnOx:D identifies the stoichiometric deviation from the pure SnO2.

The dominant diffraction peak in ($37.50^{o} < 2\theta < 40.00^{o}$) region for the SOF material in Figure 1 was attributed to the fluorine dopant. The similar condition was reported for SnOx:F sprayed films [8]. But, such peak was drastically reduced in SOF conversion to SOF C2.5. One possible explanation for this would be the competition between the Cu and F atoms to occupy the vacancy sites in SnOx:D. As observed in Figure 1, the higher quantity of Cu atoms tends to induce the decrease in all peaks.

b) SEM

XRD has identified that the atomic arrangement of atoms in the sprayed films tends to form structures similar to the stoichiometric oxides structures of SnO2 and Sn4OF6 [SnO:(SnF2)3]. However, since the interfacial transfer process depends on the surface properties, SEM and energy-dispersive spectroscopy (EDS) were used to characterize the morphology and atoms distribution on the surfaces of the sprayed films. SEM images for a set of sprayed film samples are represented in Figure 2.

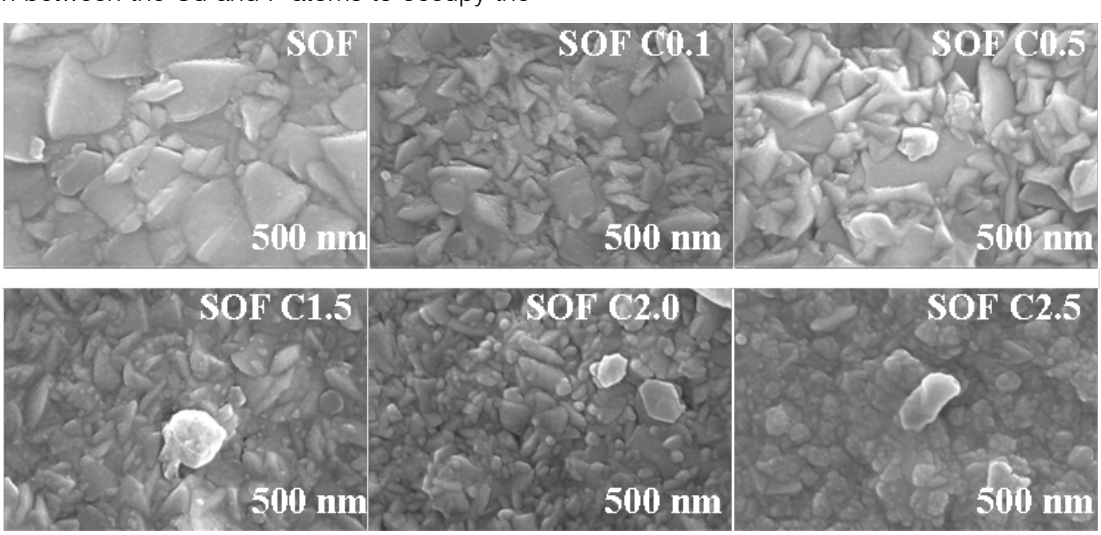

Figure 2: MEV images on the SOF and SOFC samples

For the SOF sample as a reference, from the MEV images can be inferred that the surface morphology of the products was altered when the mass of copper salts in the spray solution was increased from 0.10 g (SOF C0.1) to 2.50 g (SOF C2 .5). This change in morphology, which grains tend to decrease and become more compact, influenced the XRD profile (Figure 1). From EDS measurements, Cu atoms in the surface of SOFC materials were detected only for the SOF C2.5 sample, while the F atoms were detected in the surface of SOF and SOFC materials.

The sprayed films have heterogeneous growing, that is, material growth on a support. There is three possible paths for heterogeneous growth: overlapping uniform layers (Frank-van der Merwe), islands or agglomerates (Frank-van der Merwe) and layers and islands mixture (Stranski-Krastanow) [2,45]. Figure 3 illustrates the substrate/sprayed film interfaces obtained by SEM images. The sprayed SOF and SOFC films have the dominant Stranski-Krastanow growing.

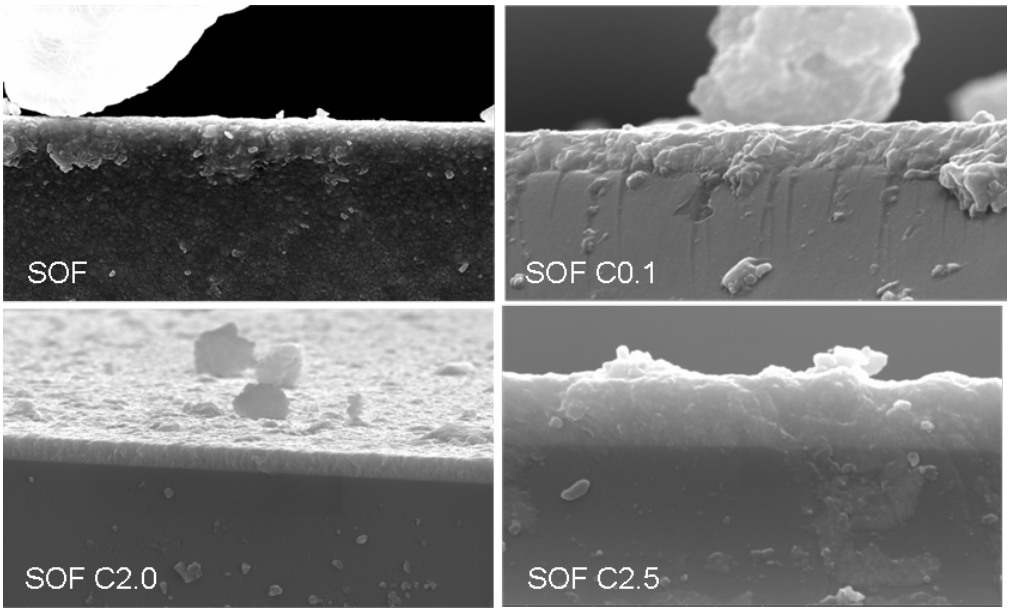

Figure 3: Substrate/sprayed film interfaces for the SOF and SOFC samples

The growing mechanisms of Frank-van der Merwe, Stranski-Krastanow and Volmer-Weber are complexes, but they are a function of the solution composition, driven thermodynamics, growing temperature and others [2, 45]. The observed growing type in SOF and SOF sprayed films was attributed to be a function of the deposition process adopted. The clusters happen when the bond energy between the superficial atoms and its neighborhood is stronger than between the atoms and the bulk layer.

c) Mott-Schottky electrochemical technique using electrochemical cell

The SnO2 films with both stoichiometric deviation and fluorine into its structure were characterized by the Mott-Schottky (M-S) technique, reporting as a n-type direct transition semiconductor [44] The n-type semiconductor has electron excess in the conduction band (CB), while the p-type presents holes excess in the valence band (VB) [1, 2, 46, 47]. As the SOFC materials have F and Cu atoms, the M-S electrochemical technique was used to identify the semiconductor type formed as a function of copper presence (Figure 4).

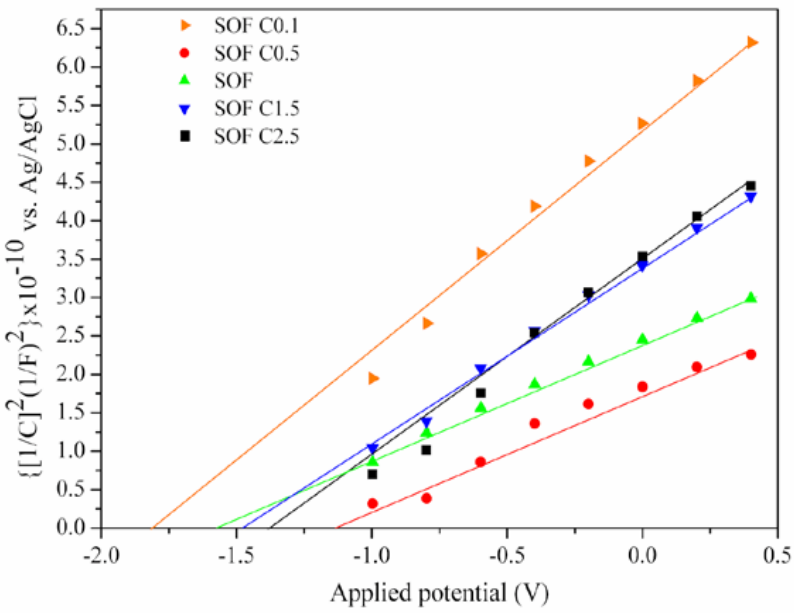

Figure 4: M-S plots for SOF e SOFC samples

Figure 4 illustrates the data obtained by M-S for the SOF and SOFC (C0.1, C0.5, C1.5 and C2.5) samples, which reflects the variation in the amount of copper atoms present in the sprayed films. The data described in Figure 3 shows that the variation of capacitance (C) of the semiconductor/electrolyte junction as a function of the applied potential (E) is a straight plot, which is typical of the M-S behavior. The SOF sample was used as standard reference.

The capacitance is typically a function of frequency (f) and the E. High frequency values have been used to eliminate the frequency influence on the capacitance in M-S plots [36,43]. The 1/C2 against E plots were generated using 1000 Hz as reference frequency [40, 42]. The illustrated data in Figure 4 was obtained for the 1000 Hz reference frequency. The slope of the straight lines (Figure 4) indicates the SOF and SOFC as n-type semiconductors. Table 2 illustrates the estimated flat-band potential (Efbp) values for the SOF and SOFC obtained from the line extrapolation forward the E axis.

Table 2: E_{fbp} and CB edge for the SOF and SOFC samples

Nº	NOMENCLATURE	E_{fbp} (V *vs* Ag/AgCl)	CB edge (eV *vs vacuum*)
1	SOF	-1.57	- 3.09
2	SOF C0.1	-1.82	- 2.40
3	SOF C0.5	-1.12	- 3.10
4	SOF C1.5	-1.45	- 2.77
5	SOF C2.5	-1.37	- 2.85

In the charge transfer process in the titanium dioxide (TiO2)/SnO2 junction, the Efbp values of materials obtained by M-S plots were assumed to be an approximate measurement of the CB edge of a n-type semiconductor [39]. Table 2 shows the CB edge values determined from Efbp values and converted to the absolute energy scale (vacuum). The CB edge change as a function of the copper atoms identifies an electronic distribution change into the CB of SOF and SOFC materials.

Regarding the materials from the SOFC group, the Cu atoms in the matrix seem to have contributed to the shift of Efbp to less negative values, but a non-linear increase of electrons in the CB, results in the shift of the CB edge. Such behavior is admissible, once the materials exhibit the n-type semiconductor behavior, which is associated with the electrons excess in the CB. In the CuFeO films, doped with calcium atoms, it was reported Efbp increase with the increment of the calcium (Ca) dopant from the Efbp= +0.70 V, for the pure film, and reaching Efbp= +0.93 V at 10% doping [40].

The Efbp value changes with the electrolyte composition. The increment in the Efbp value contributes to increase the charge transfer through the semiconductor/electrolyte junction [43]. Also, The Efbp interferes with the photovoltaic behavior of the DSSCs [20,23]. In TiO2-based dye-sensitized solar cells (DSSCs), the doping by ferric (Fe) dislocated the Efbp value to more positive potentials, Efbp (TiO2) = -0.73 V became Efbp (TiO2:Fe) = -0.55 V, and it increased the

efficiency of the cell due to the good charge separation between TiO2:Fe CB and the LUMO of dye [23].

For the SnOx:F/CuFeO2/dye/redox and (I-/I3-)/Pt-SnOx:F sandwich structure DSSC, the value of the open circuit voltage (Voc) was estimated from Efbp(CuFeO2) and Eredox(I-/I3-) using Voc = Efbp(CuFeO2) - Eredox(I-/I3-) [20]. From the Efbp(CuFeO2) the value converted to the standard hydrogen electrode (SHE) electrochemical scale and Eredox(I-/I3-) = + 0.32V vs SHE, was then Voc= 0.37 V, while the experimental value was 0.365 V. The Efbp (CuFeO2) value was estimated by M-S measurement in a 1.0 M NaOH solution with the aid of silver/silver chloride (Ag/AgCl) as reference electrode.

In relation to the dye-sensitized solar cells (DSSCs), the literature has reported that the theoretical Voc can be estimated from Voc = ECB - Eredox, where ECB is CB edge position of semiconductor. From this methodology, it is possible to infer that the approximation ECB~Efbp for the n-type semiconductor, which is a good tool in the characterization of materials for photovoltaic applications. Besides the knowledge on structural, morphologic and electronic properties of semiconductors, it is also important to determine the electrical and optical properties to understand the role they play in the photovoltaic field.

d) Sheet resistance (Rs)

SnO2 is an n-type semiconductor in which the presence of oxygen vacancies, cations and anions as dopants are responsible for the conductivity generated by the electrons transport [1]. SnO2 films synthesized by spray pyrolysis technique have been doped using manganese (Mn) [11], copper (Cu) [12] and chromium (Cr) [13] as source of cations doping. Titanium (Ti), zinc (Zn), tin (Sn), Cu, Mn, Cr and others are atoms that tend to form electrical insulating oxides [1]. Thus, research generally approached the influence of these atoms only as dopants on properties of bulk oxides.

For electrical characterization, the sheet resistance (Rs) has been used to measure the electrical resistance of materials in films. The two points method was reported for electrical characterization of SnOx:F films to the Rs measurement [5]. The sheet resistance (Rs) is the more adequate characterization for films due to the large area of the films that favors the capture of electrons by superficial defects [48].

In SnOx: F films from spray pyrolysis, Rs values were reported between 107.9 Ω/□ to 17.8 Ω/□ [5]. These values were obtained using the two points method with the aid of a digital multimeter. Table 3 illustrates the Rs values of the sprayed films determined by the two points method. For 35.80Ω/ □ to 17.60Ω/ □ (Table 3), the values agree with the ones reported for Rs of SnOx: F films obtained from the two points method [5].

The Rs values described in Table 3 reflects the dependence on the work conditions. For the SOF materials as referenced in Table 3, the increased number of copper atoms in sprayed films causes an obvious change in the resistance, which can be due to the transition from conductive to insulate phase or loss of oxygen vacancies or low F atoms into the SnOx: F matrix. A decrease in the number of oxygen vacancies, in SnO2 thin films, during the deposition, results in a reduction of the charge transporter concentration and, therefore, of the electrical conductivity [1]. In the self-doping of SnO2, the oxygen vacancies responsible for the electrical conductivity are occupied by the Sn+2 ions [32].

Table 3: R_s values of sprayed films by the two points method

Nº	Nomenclature	R_s (Ω/□)
1	SOF	17.60
2	SOF C0.1	20.20
3	SOF C0.2	24.50
4	SOF C0.3	24.60
5	SOF C0.4	24.90
6	SOF C0.5	20.70
7	SOF C1.0	25.70
8	SOF C1.5	28.40
9	SOF C2.0	35.00
10	SOF C2.5	35.80

From another approach, the increase in the Rs, with copper increase, is associated with the decrease of the prominent diffraction peak in $37.5^{o} < 2\theta < 40^{o}$ interval (Figure 1), morphology change in Figure 2 and formation of islands in Figure 3. Through transmission electron microscopy (TEM), it was found that the excess of antimony (Sb) dopant in the semiconductor creates agglomerates that increase the material electrical resistance [49]. The effects of copper atoms on the optical and structural properties of the SnO2 films have been reported [12], leaving out the electrical properties. Probably, the electrical characterization has not been mentioned previously because copper tends to make electrical insulators such as oxides.

From the electrical measurements in Table 3, it can be inferred that the copper (Cu) atoms act opposite to fluorine (F) atoms. By the size, the proximity of the F-ion with the O2- ion, the F- ions occupies the sites emptied by the oxygen absence [32]. Additionally, the antimony (Sb) ions, by being larger than the F-, substitute the tin atoms ions [8]. The electrical transparent conductors based in tin oxides made by spray pyrolysis presented Rs higher with Sb than with the F dopant [8]. Similarly to the Sb atoms, the Cu atoms in the SOFC can substitute the tin atoms in the tin sites (Sn+4 or Sn+2 or both) into the SnOx:F matrix.

Taking in consideration the crystal net, fluorine is a dopant which contributes to minimize Rs, because it causes less net deformation than copper. Copper increments Rs due to the deformation caused in the net. This decrease probably happened due to the diminution

in the quantity of extinct vacancies or increase in the quantity of generated agglomerates or both. The decrease of the peaks of diffraction (Figure 1) is the result of this behavior.

Not only the type of doping, also the process conditions affect Rs. The SnOx:F films obtained by spray pyrolysis at 400 °C from a solution mixture of acid, tin and fluorine salts presented Rs between 38.02 Ω/□ to 300.02 Ω/□ [6]. The SnOx:molybdenum (Mo) films produced by spray pyrolysis at 500 °C resulted in Rs between 39.81 Ω/□ to 98.23 Ω/□, while the pure phase had Rs equals to 109.81 Ω/□ [10].

Additionally, the spray pyrolysis is a technique capable of induce oxygen vacancies into oxides. It is a useful tool in the preparation of doped and pure oxide films with stoichiometric deviation from spray solutions with the salts and acids. This research showed that the spray solutions without the addition of acids produced materials with Rs varying between 20.20 Ω/□ up to 35.80 Ω/□. These values agree with data reported in literature.

e) Transmittance, thickness and band gap from optical spectroscopy

The optical transmittance is one characterization technique that can be used in the study on the behavior of materials on ultraviolet-visible-infrared radiations. Figure 4 illustrates the transmittance of the samples SOF C1.5, SOF C2.0, SOF and bare glass into ultraviolet-visible radiations. From Figure 5, the transmittance of SOFC materials can be compared to the SOF matrix and bare glass transmittance. The presence of copper (Cu) atoms seems to affect the SOF matrix transmittance both decreasing (SOF C2.0) and increasing (SOF C1.5).

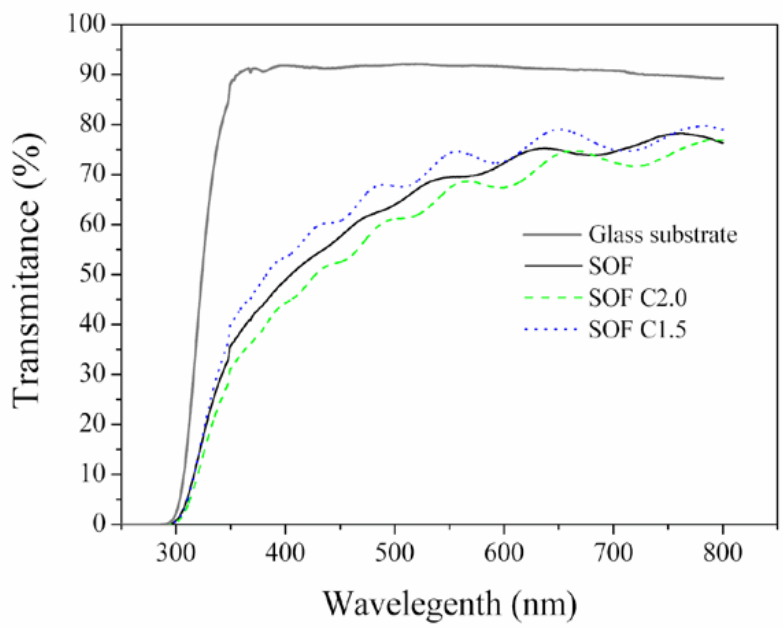

Figure 5: Optical transmittance values for samples SOF and SOFC

The transmittance value for SOF reaches close to 80% only at about λ = 800 nm, but transmittance decreases when the λ downwards, reaching values below 60% for λ < 500 nm. This behavior is similar for SOFC materials. For SOF matrix as reference, the increment in the SOF C1.5 can be attributed to a random distribution of copper atoms in the matrix. Such distribution may have helped to minimize the formation of agglomerates or impurities that induce the transmittance loss. The agglomerates were identified in SOF and SOFC materials (Figure 3).

The loss of transmittance in relation to the glass substrate may be related to a higher proximity between the atoms in the matrix. This approximation may have caused agglomerates capable of inducing absorption or reflection of the visible radiation or the incident luminous energy. Therefore, the transmittance seemingly increased when sprayed by a copper(II) chloride dihydrate (1.50 g) solution, which provides SOF C1.5 (Table 1). Possibly, the increase in transmittance was caused by a more efficient random distribution of copper atoms in the matrix with grains decreasing (Figure 2).

The loss of transmittance in a material can be attributed to the reflection and/or absorption phenomenon [50]. As mentioned previously, the film's dominant growth was Stranski-Krastanow. Possibly, the type of growth caused some loss in the transmittance. In the other side, in the SnOx:F from the spray pyrolysis technique, SnO, HF, SnF4 transitory composites are formed during the process and, due to the temperature effect, react with oxygen to form the SnOx: F product

[8]. Therefore, such transitory composites can be present in the SOFC materials as impurities acting to reduce the transmittance. From XRD (Figure 1), it was estimated the possible presence of SnF2 in SOF and SOFC materials.

Figure 5 illustrates peaks and valleys (interference fringes) in the optical transmittance spectrum. The peaks and valleys in the optical transmittance spectrum of film/substrate junction reflect a layer adherent to the substrate [34]. Also, the peaks and valleys generated in the spectrum of optical transmittance on a film/substrate junction have been used to estimate the film thickness (t) and band gap (Eg) [5,7].

The advantage of the optical characterization is the possibility of determining the t and Eg using only transmittance data. Table 4 shows the values for t and Eg for spayed materials, obtained only from optical characterization. The t values for SOF and SOFC materials were estimated through Equations 4-7, while the Eg values were specified using the Tauc relation, Equations 2 and 3.

Table 4: The t and E_g values of the SOF and SOFC materials

Nº	NOMENCLATURE	t^{op} (nm)	E_g^{op} (eV)
1	SOF	643.36	3.15
2	SOF C0.1	636.68	3.10
3	SOF C0.2	658.58	3.37
4	SOF C0.3	621.26	3.22
5	SOF C0.4	647.54	3.00
6	SOF C0.5	658.57	3.37
7	SOF C1.0	647.67	3.30
8	SOF C1.5	676.53	3.47
9	SOF C2.0	641.43	3.32
10	SOF C2.5	653.55	3.52

The random distribution of copper atoms (Cu), the preparation process and measurement conditions seemingly have influenced non-linear behavior of Eg (Table 4). The Eg variation as function of the preparation conditions and doping has been reported in literature. The Eg change on tin oxide materials was 4.0 eV for monolayer and 1.16 eV for three layers of deposited film [51]. Antimony (Sb), as the dopant, injects free electrons in the conduction band of the tin oxide, which causes an increase on the Eg [1] SnO2 films, Eg = 3.911 eV, while Eg = 4.011 eV with the increment of molybdenum (Mo) atoms in the matrix [10].

For semiconductors that behave as electrical conductors, the electronic conductivity is due to the oxygen vacancies and presence of electrons or holes from dopants into the energy bands of semiconductors. A transparent semiconductor as electrical conductor is a material with high electrical conductivity and band gap (Eg) higher than 3.10 eV (Eg > 3.10 eV) that provides low absorption in the visible solar radiation [1].

The inorganic semiconductors have the conduction band (CB) and valence band (VB) energy levels, while organic semiconductors have LUMO and HUMO, equivalent to CB and VB, respectively. The optical Eg and electrochemical HOMO values from the LUMO = HOMO + Eg were used to obtain LUMO [10]. Figure 6 shows the BC and VB edge position of the SOF and SOFC being as function of copper and obtained from the CB = VB + Eg, where CB is assumed as Efbp (Table 2) and Eg is illustrate in Table 4.

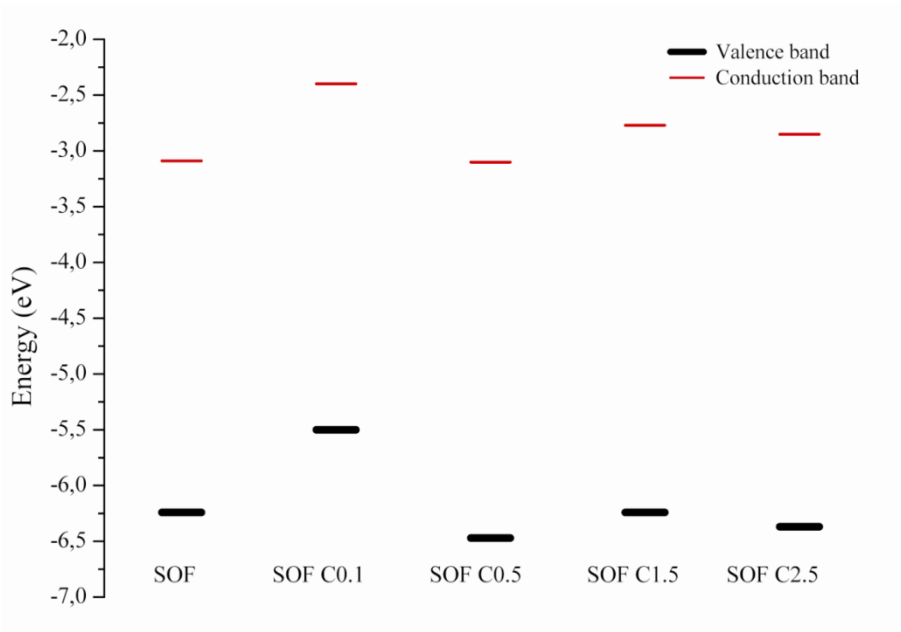

Figure 6: CB and VB edges for samples SOF and SOFC

By previously exposed information about SOF and SOFC materials, it is possible to attribute that these materials are n-type semiconductors oxides, as well as transparent and electrical conductors and Eg > 3.10 eV. Once those photovoltaic solar cells use the visible region to generate electricity, the SOF and SOFC materials have potential for photovoltaic applications as collectors of electrons or in the form of conductor transparent oxide or counter electrode. Therefore, the SOF and SOFC materials were used in DSSCs as being SOF/platinum and SOFC/platinum counter electrodes.

f) Dye-sensitized solar cell (DSSC)

In DSSCs, the photovoltaic effect occurs by electron transfer at the surfaces of electrodes, the photoanode and counter electrode, from the photo electrochemical reactions. These reactions involve the charge transfer at the electrode surface, the electrolyte resistance, mass transfer from the electrolyte to the electrode surface and the electroactive species adsorption. The DSSC photovoltaic characteristics results from the net amount of the electron transfer processes into the cell. Figure 7 shows the photocurrent density-voltage (J-V) characteristics for DSSC with various photoanodes under a simulated solar light about 100 mW/cm2.

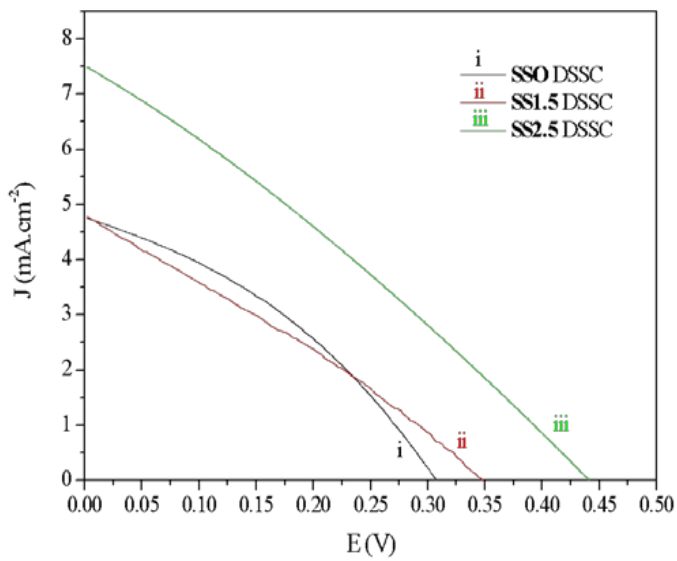

(a)

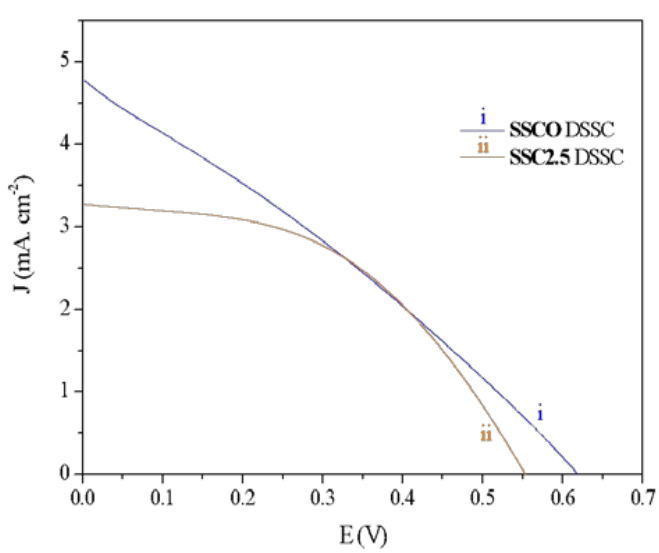

(b)

Figure 7: J *vs* V plots for the DSSCs: a) SnO_2 photoanodes and b) SnO_2:CuO photoanodes

All photovoltaic parameters are shown in Table 5. As Rserial is a resistance ohmic setup and Rshunt represents the setup of resistance to charge recombination in DSSC, then for ideal solar cell Rserial << Rshunt. Moreover, the results illustrated in Figure 7 and Table 5 are attributed to the effective influence of Rserial > Rshunt.

The fill factor (FF) indicates cell stability in face of energy generation. FF is given by a ratio between the maximum energy product (J.V)max and the ideal energy product (Jsc.Voc).Therefore, the closer FF is to one, the higher is the cell stability under luminous energy presence. The cell stability represents resistance to energy loss, which occurs when the cell is submitted to an electrical field induced by charge accumulation space (CAS), under the presence of the luminous energy.

Table 5: Photovoltaic parameters at 100 mW/cm^2 by various photoanodes of DSSC devices

Photoanode	DSSC	V_{oc}(V)	J_{sc} (mA/cm^2)	FF	η(%)	R_{serial} (Ω.cm^2)	R_{shunt} (Ω.cm^2)
SOF/SnO_2	SS0	0.31	4.75	0.36	0.52	1303.00	996.10
SOF C1.5/SnO_2	SS1.5	0.35	4.78	0.29	0.48	1113.80	993.50
SOF C2.5/SnO_2	SS2.5	0.44	7.49	0.28	0.93	1139.70	995.60
SOF/SnO_2:CuO	SSC0	0.62	4.77	0.29	0.86	1052.50	995.30
SOF C 2.5/ SnO_2:CuO	SSC2.5	0.55	3.28	0.48	0.86	1084.30	998.30

The low values of FF illustrated in Table 5 show high electrons concentration with lower energy than the electrical fields induced on SnO2 based photoanodes. But, the FF and Jsc values follow the literature for modified and unmodified SnO2 nanoparticles based photoanodes. For example, Jsc =2.45 mA/cm2 and FF = 0.5404 SnO2 photoanode [26]. Jsc =4.80 mA/cm2 and FF = 0.308 SnO2:ZnO photoanode [27], Jsc =9.2 mA/cm2 and FF = 0.332 SnO2 photoanode [30].

Among DSSCs, SS2.5 DSSC has an obvious increase in current density (Jsc) and open circuit voltage (Voc). But, photoelectrons have lower energy than the electrical fields induced by charge accumulation space into the solar cell, which from a specified voltage is captured by the charge accumulation space instead of the electron's acceleration. This process influences low Rshunt, high Rserial and low FF. Subsequently, the SnO2-CuO mixture on the SOF C 2.5 for the SSC2.5 DSSC provides Rshunt and FF higher than that of SS2.5 DSSC.

V. Conclusion

Copper decorated fluorine doped tin oxide films and its application in the photovoltaic performance of DSSCs was investigated in this study. From the characterizations, it is possible to assume that the properties of the material synthesized by the spray pyrolysis were influenced by copper concentration. However, the material keeps its characteristic as a transparent electrical conductor oxide. The composition of copper decorated fluorine doped tin oxide also facilitates the enhancement of the photocurrent and Jsc, and improves energy conversion efficiency of the DSSCs.

Acknowledgments

The authors gratefully acknowledge the Universidade Federal do Ceará, which provided the necessary facilities to complete this work. Also, the Fundação Cearense de Apoio ao Desenvolvimento Científico e Tecnológico (FUNCAP), Conselho Nacional de Desenvolvimento Científico e Tecnológico (CNPq) and Coordenação de Aperfeiçoamento de Pessoal de Nível Superior (CAPES) by research and education support in the Brazil.

Declaration of Conflicting Interests

The author(s) declared no potential conflicts of interest with respect to the research, authorship, and/or publication of this article.

References Références Referencias

1. Ginley DS, Hosono H and Paine DC. Handbook of Transparent Conductors, first ed., Springer, New York; 2010.
2. Kosyachenko LA . Solar Cells: New Aspects and Solutions, first ed., InTech, Rijeka; 2010.
3. Maia Jr PHF, Lima FM, de Sena AC, Silva ÁN, Martins FM, Almeida AFL and Freire FNA. Deposition by spray-pyrolysis of tin oxide doped with fluorine produced by sol-gel method. Mater. Sci. Forum. 2016; 869:977-981.
4. Alkhayatt AHO and Hussian SK. Fluorine highly doped nanocrystalline SnO2 thin films prepared by SPD technique, Mater. Lett. 2015; 55:109-113.
5. Supriyono, Surahmana H, Krisnandia YK and Gunlazuardia J.Preparation and characterization of transparent conductive SnO2-F thin film deposited by spray pyrolysis: relationship between loading level and some physical properties, Procedia Environment. Sci. 2015; 28:242-251.
6. Jafar AM, Al-Amara K, Rashid FL and Fayyadh IK. Fabrication and characterization of fluorine-doped tin oxide transparent conductive nano-films, IJIRST 2013; 6:49-58.

7. Tatar D, Turgut G and Düzgün B. Effect of substrate temperature on the crystal growth orientation and some physical properties of SnO2:F thin films deposited by spray pyrolysis technique, Rom. Journ. Phys. 2013; 58:143-158.
8. Elangovan E and Ramamurthi K. A study on low cost-high conducting fluorine and antimony-doped tin oxide thin films, Appl. Surf. Sci. 2005; 249:183-196.
9. Banyamin ZY, Kelly PJ, West G and Boardman J. Electrical and optical properties of fluorine doped tin oxide thin films prepared by magnetron sputtering. Coatings 2014; 4: 732-746.
10. Turgut G and Sönmez E. Synthesis and characterization of Mo doped SnO2 thin films with spray pyrolysis, Superlattices Microstruct. 2014; 69:175-186.
11. Vadivel K, Arivazhagan V and Rajesh S. Mn doped SnO2 semiconducting magnetic thin films prepared by spray pyrolysis method, IJSER 2011; 2:1-5.
12. Roy SS and Podder J. Synthesis and optical characterization of pure and Cu doped SnO2 thin films deposited by spray pyrolysis, J. Optoelectron. Adv. M. 2010; 12:1479-1484.
13. Kasar RR, Gosavi SR, Ghosh A, Deshpande NG and Sharma RP. Influence of Cr doping on structural, morphological and optical properties of SnO2 thin film prepared by spray pyrolysis technique, OSR-JAP 2015; 7:21-26.
14. Prima EC, Hidayat NN, Yuliarto B, Suyatman and Dipojono HK. A combined spectroscopic and TDDFT study of natural dyes extracted from fruit peels of Citrus reticulata and Musa acuminata for dye-sensitized solar cells, Spectrochim. Acta A 2017; 171: 112-125.
15. Guo M, Yao Y, Zhao F et al. An In 2.77S4 @conductive carbon composite with superior electrocatalytic activity for dye-sensitized solar cells, J. Photochem. Photobiol. A. 2017; 332:87-91.
16. Bendoni R, Barthélémy AL, Sangiorgi N, Sangiorgi A, Sanson A. Dye-sensitized solar cells based on N719 and cobalt gel electrolyte obtained through a room temperature process, J. Photochem. Photobiol. A. 2016; 330:8-14.
17. Chu L, Qin Z, Liu W, Ma X. Inhibition of charge recombination for enhanced dye-sensitized solar cells and self-powered UV sensors by surface modification, Appl. Surf. Sci. 2016; 389:802-809.
18. Maçaira J, Andrade L and Mendes A. Laser sealed dye-sensitized solar cells: Efficiency and long term stability, Sol. Energy Mater. Sol. Cells 2016; 157:134-138.
19. Maurya IC, Srivastava P and Bahadur L. Dye-sensitized solar cell using extract from petals of male flowers Luffa cylindrica L. as a natural sensitizer, Opt. Mater. 2016; 52: 150-156.
20. Zhu T, Deng Z, Fang X et al. High photovoltages of CuFeO2 based p-type dye-sensitized solar cells, J. Alloys Compd. 2016; 685:836-840.
21. Park KH, Kim SJ, Gomes R and Bhaumik A. High performance dye-sensitized solar cell by using porous polyaniline nanotubes as counter electrode, Chem. Eng. J. 2015; 260:393-398.
22. Tsai CH, Fei PH and Wu WC. Enhancing the efficiency and charge transport characteristics of dye-sensitized solar cells by adding graphene nanosheets to TiO2 working electrodes. Electrochimic. Acta 2015; 165:356-364.
23. Liu QP. Analysis on dye-sensitized solar cells based on Fe-doped TiO2 by intensity-modulated photocurrent spectroscopy and mott-schottky, Chin. Chem. Lett. 2014; 25:953-956.
24. Duong TT, Tuan TQ, Dung DVA et al. Application of polyaniline nanowires electrodeposited on the FTO glass substrate as a counter electrode for low-cost dye-sensitized solar cells, Curr. Appl. Phys. 2014; 14:1607-1611.
25. Skupien K, Putyra P, Walter J, Kozłowski RH, Khelashvili G, Hinsch A and Würfel U.Catalytic materials manufactured by the polyol process for monolithic dye-sensitized solar cells, Prog. Photovolt: Res. Appl. 2009; 17:67-73.
26. Arote SA, Tabhane VA and Pathan HM. Enhanced photovoltaic performance of dye sensitized solar cell using SnO2 nanoflowers, Opt. Mater. 2018; 75:601- 606.
27. Bu IYY. Novel ZnO decorated SnO2 nanosheet for dye sensitized solar cell applications, Optik 2018; 157:406-409.
28. Asemi M and Ghanaatshoar M Hydrothermal growth of one-dimensional Ce-doped TiO2 nanostructures for solid-state DSSCs comprising Mg-doped CuCrO2, J Mater Sci 2017; 52:489 - 503.
29. Iqbal MZ and Khan S. Progress in the performance of dye sensitized solar cells by incorporating cost effective counter electrodes, Sol. Energy 2018; 160:130 - 152.
30. Shaikh SF, Manea RS and Joo OS. Spraying distance and titanium chloride surface treatment effects on DSSC performance of electrosprayed SnO2 photoanodes, RSC Adv. 2014; 4:35919 - 35927.
31. Chua L, Qinc Z, Liuc W and Mad X. Inhibition of charge recombination for enhanced dye-sensitized solarcells and self-powered UV sensors by surface modification, Appl. Surf. Sci. 2016; 389:802 - 809.
32. Hass G, Francóme HM and Vossen JL, Physics of Thin Films: Advances in Research and Development, twelve ed., Academic Press, New York; 1982.
33. Girotto EM and Santos IA. Medidas de resistividade elétrica dc em sólidos: como efetuá-las corretamente, Quim. Nova 2002; 25:639-647.

34. Adawiya JH, Shaker SS and Mohammed AH. A study of morphological, optical and gas sensing properties for pure and Ag doped SnO2 prepared by pulsed laser deposition (PLD), Energy Procedia 2013; 36:776-787.
35. Xu Y, Hou LY and. Zhang XM. Zinc tin oxide thin films prepared by MOCVD with different Sn/Zn ratios, Rare Metals 2017; 36:753 - 757.
36. Fernández-Domene RM, Sánchez-Tovar R, Sánchez-González S and García-Antón J. Photo-electrochemical characterization of anatase-rutile mixed TiO2 nanosponges, Int. J. Hydrog. Energy 2016; 41:18380-18388.
37. Cotfas DT, Cotfas PA and Kaplanis S.Methods and techniques to determine the dynamic parameters of solar cells: Review, Renew. Sust. Energ. Rev. 2016; 61:213-221.
38. Jarosz G. On doubts about Mott-Schottky plot of organic planar heterojunction in photovoltaic cell, J. Non-Cryst. Solids 2008; 354:4338-4340.
39. Ramírez-Ortega D, Acevedo-Penã P, Tzompantzi F, Arroyo R, González F and González I. Energetic states in SnO2 - TiO2 structures and their impact on interfacial charge transfer process, J Mater Sci. 2017; 52:260 - 275.
40. Xiong X, Zhang Q, Verma SK, Bao XQ, Li H and Zhao X. Crystal structural, optical properties and mott-schottky plots of p-type Ca doped CuFeO2 nanoplates, Mater. Res. Bull. 2016; 83:141-147.
41. Brus VV, Kyaw AKK, Maryanchuk PD and Zhang J. Quantifying interface states and bulk defects in highefficiency solution-processed small-molecule solar cells by impedance and capacitance characteristics, Prog. Photovolt: Res. Appl. 2015; 23:1526-1535.
42. Ren C, Wang W, Jin X, Liu L and Shia T. Physicochemical performance of FeCO3 films influenced by anions. RSC Adv. 2015; 5:20302-20308.
43. Karazehir T, Ates M and Sarac AS. Mott-Schottky and morphologic analysis of poly(pyrrole-N-propionic acid) in various electrolyte systems International, Int. J. Electrochem. Sci. 2015; 10:6146-6163.
44. Fabregat-Santiago F, Garcia-Belmonte G, Bisquert J, Bogdanoff P and Zaban A. Mott-Schottky analysis of nanoporous semiconductor electrodes in dielectric state deposited on SnO2(F) conducting substrates, J. Electrochem. Soc. 2003; 150:E293-E298.
45. Schmickler W and E. Santos E. Interfacial Electrochemistry, second ed., Springer, New York; 2010.
46. Quaschning V. Undestanding Renewable Energy Systems, first ed., Earthscan, London; 2005.
47. Goswanami DY, Kreith F and Kreider J.F. Principles of Solar Engennering, second ed.,Taylor & Francis Group, New York; 2000.
48. Razeghi M. Fundamentals of solid state engineering, first ed., Kluwer academic publishers, New York, 2002.
49. Voyles PM, Muller DA, Grazul JL, Citrin PH and Gossmann HJL. Atomic-scale imaging of individual dopant atoms and clusters in highly n-type bulk Si, Nature 2002; 416:826-829.
50. Padilha AF. Materiais de Engenharia - Microestrutura e Propriedades, first ed. Hemus, Curitiba; 1997.
51. Zhouabc W and Umezawa N. Band gap engineering of bulk and nanosheet SnO: an insight into the interlayer Sn–Sn lone pair interactions, Phys. Chem. Chem. Phys. 2015; 17:17816-17820.

ORCID
Edwalder Silva Teixeira https://orcid.org/0000-0002-6037-5985
Francisco Marcone Lima https://orcid.org/0000-0002-1898-9350
Vanja Fontenele Nunes https://orcid.org/0000-0003-2458-5616
Antonio Paulo Santos Souza https://orcid.org/0000-0002-0315-9813
Ana Fabíola Leite Almeida https://orcid.org/0000-0002-8867-5453
Francisco Nivaldo Aguiar Freire https://orcid.org/0000-0001-5449-2635